Case Studies in Thermal Engineering 24 (2021) 100843

Contents lists available at ScienceDirect

Case Studies in Thermal Engineering

journal homepage: http://www.elsevier.com/locate/csite

Effect of the blockage ratios of circular stack on the performance of the air-based standing wave thermoacoustic refrigerator using heat pipe

Praitoon Chaiwongsa [a], Somchai Wongwises [a,b,*]

[a] Fluid Mechanics, Thermal Engineering and Multiphase Flow Research Lab. (FUTURE), Department of Mechanical Engineering, Faculty of Engineering, King Mongkut's University of Technology Thonburi (KMUTT), Bangmod, Bangkok, 10140, Thailand
[b] National Science and Technology Development Agency (NSTDA), Pathum Thani, 12120, Thailand

ARTICLE INFO

Keywords:
Blockage ratio
Spiral stack
Circular stack
COP
Heat pipe
Thermoacoustic refrigerator

ABSTRACT

In this study, the coefficient of performance (COP) and relative coefficient of performance (COPR) of an air-based standing wave thermoacoustic refrigerator (ASWTAR) was investigated. All relevant components of the thermoacoustic refrigerator were fully available in the system. Heat pipes with a total heating power of 30W were installed into the cold-side and hot-side heat exchangers. The circular stacks with plugging ratios of 0.67, 0.71 and 0.74 and the spiral stacks with plugging ratio of 0.74 were tested and compared. The results show that the circular stack is the optimum stack geometry for ASWTAR. Similarly, a circular stack with a blockage ratio of 0.71 has the best performance, producing the lowest cold side temperature (T_c) and the highest temperature difference (ΔT_m). Under no cooling load and 2W cooling load, T_c, ΔT_m, COP and COPR were 22.4 °C, 30.5 °C, 0.93 and 9.57%, respectively. Finally, it is clear that due to the use of more suitable materials, the COP and COPR of a circular stack are greater than those of a spiral stack.

1. Introduction

In the development of refrigeration systems, we must first consider the impact on the environment. Refrigerants that are harmful to the environment should not be used. The development of refrigerants and alternative methods of refrigeration technology is the effort and focus of most research. One of the most interesting refrigeration technology is thermoacoustic refrigeration.

Thermoacoustic heat pumps and refrigerators use acoustic energy to pump heat from low-temperature sources and sink through porous media at high temperatures. In thermoacoustic refrigerators, environmental-friendly gases are used as operating gases. In addition to being a clean technology, this technology also has many interesting advantages, including a system with no moving parts, a simple structure, and requiring less equipment. Therefore, it has a longer estimated operating life than conventional refrigerators and requires less manufacturing and maintenance costs.

Rott [1] studied and discussed the oscillating flow on non-isothermal surfaces, the damping and excitation of gas columns, temperature stratification, and thermoacoustic flow. Hofler [2] built a fully functional thermoacoustic refrigerator in which the lowest ratio of the cold side temperature to the ambient temperature was 0.66, and the highest COPR of the temperature ratio was 12% at 0.82 temperature ratio. Swift [3] reviewed and introduced the principle fundamentals through analysis and examples of thermoacoustic

* Corresponding author. National Science and Technology Development Agency (NSTDA), Pathum Thani, 12120, Thailand.
E-mail address: somchai.won@kmutt.ac.th (S. Wongwises).

https://doi.org/10.1016/j.csite.2021.100843
Received 30 July 2020; Received in revised form 20 October 2020; Accepted 4 January 2021
Available online 7 January 2021

Nomenclature

ASWTAR	air-based standing wave thermoacoustic refrigerator
A	cross section area (m^2)
A_s	surface area of heat transfer (m^2)
a	speed of sound (m s^{-1})
B	blockage ratio (dl)
CHX	cold side heat exchanger
COP	coefficient of performance (dl)
COPc	Carnot's coefficient of performance (dl)
COPR	relative coefficient of performance (dl)
CSE	cold side end of stack
c_p	isobaric specific heat of working gas (J $kg^{-1}K^{-1}$)
cs	circular stack
c_s	specific heat of stack material (J $kg^{-1}K^{-1}$)
D	drive ratio (dl)
dl	dimensionless
D_r	resonator diameter (m)
E_i	electrical input voltage (V)
η_s	efficiency of loudspeaker (dl)
f	operating frequency (Hz)
h	height of resonator cone (m)
HP	heat pipe
HPHX	heat pipe heat exchanger
HSE	hot side end of stack
HHX	hot side heat exchanger
I_i	electrical input current (A)
k	thermal conductivity (W m^{-1} K^{-1})
K	wave number (m^{-1})
l_0	half of stack layer thickness (m)
L_s	stack length (m)
L_{sn}	normalized stack length (dl)
L_t	resonator length (m)
M	Mach number (dl)
P_i	electrical input power (W)
PF	power factor
PLA	polylactic acid
PVC	polyvinylchloride
p_0	dynamic pressure amplitude (Pa)
p_m	mean pressure (Pa)
Q_c	cooling power (W)
Q_{cn}	normalized cooling power (dl)
Re	Reynolds number (dl)
ss	spiral stack
TAR	thermoacoustic refrigerator
TEM	thermoelectric module
T_c	cold side temperature of stack (°C)
T_h	hot side temperature of stack (°C)
T_m	mean temperature (°C)
u	velocity (m s^{-1})
W	acoustic power (W)
W_n	normalized acoustic power (dl)
WCS	water cooling system
X_s	stack center position (m)
X_{sn}	normalized stack center position (dl)
y_0	half of distance between the stack layer (m)
δ_k	thermal penetration depth (m)
δ_{kn}	normalized thermal penetration depth (dl)
δ_v	viscous penetration depth (m)
γ	ratio of specific heat (dl)

engines.

Garrett et al. [4] built a thermoacoustic refrigerator like a small domestic refrigerator, with a cooling capacity of 120W at −22 °C and a 200W at 4 °C, intended for use in Space Shuttle Discovery. Swift [5] introduced the basics of thermoacoustic engines and refrigerators, commercial development, and the power and efficiency of devices. Wetzel and Herman [6] evaluated and optimized the stack performance, using the short stack boundary layer approximation method. However, this simplified linear model was not suitable for the design and optimization purposes.

Belcher et al. [7] reported that low Prandtl number and high specific heat ratio were characteristics of the best operating gas. The gas performance must be optimized for specific application and it cannot be extrapolated that a low Prandtl number and a high specific heat ratio are always required. Poese and Garrett [8] used a linear acoustic computer model to measure the acoustic power deviation of the thermoacoustic refrigerator. The results show that at 3% and 6% of the drive ratio, the deviation of the acoustic power was about 8% and 24%, respectively. Tijani et al. [9] designed a thermoacoustic refrigerator by using a short stack boundary layer approximation for heat flow and acoustic power. They could reduce many design parameters by choosing some parameters and using dimensionless parameters.

Tijani et al. [10] constructed and tested the performance of thermoacoustic refrigerators and found a low temperature of −65 °C, which was one of the lowest temperatures reported to date. Herman and Chen [11] improved the simplified heat transfer model to study the thermal behavior of stack plates and heat exchangers. They used flat tubes and the fluid circulated in the tubes without causing a blockage. Akhavanbazaz et al. [12] studied the effect of gas blockage on small and large surface area heat exchangers. In all cases, the blockage ratio was found to have a direct effect on the thermoacoustic process. Nsofor and Ali [13]tested and compared the performance of certain parameters under critical conditions. The results showed that when the cooling load increases, the temperature difference also increased. At the optimal pressure and frequency, the thermoacoustic refrigeration system should be operated to obtain the highest cooling load.

Tasnim et al. [14] investigated the effects of variation on operating fluids and operating conditions using a thermoacoustic numerical model. The results of the study indicate that reducing the Prandtl number of the gas will not improve performance. With a drive ratio of 0.017, for half the stack spacing of $3.33\delta_k$, by reducing the Prandtl number from 0.7 to 0.28, the COP increases by 78%. When the drive ratio is 0.017, the stack spacing is half of $1.0\delta_k$, and COP is reduced by reducing the Prandtl number from 0.7 to 0.28. Good agreement is found when compared with the experimental results.

Nayak et al. [15] tested and compared the performance of TAR in terms of stack geometry and materials. It is found that the temperature difference is the largest when the cooling load is 2W and the frequency is 400 Hz. At a mean pressure of 10 bar and a cooling load of 2W, the temperature difference of the parallel plate stack is 19.4 °C (used as a Mylar material) and is larger than other stack geometries.

Yahya et al. [16] tested and studied the performance of ASWTAR. The stack with three types of random materials (scrap metal) were tested and compared. In addition, a parallel plate stack made of a stainless steel plate and Mylar plate was used as a reference test case. The results clearly show that Mylar plates stack have better performance than the other stack. There is a temperature difference. The highest COP and COPR are 7.7 °C, 0.217 and 0.15%, respectively. Finally, the results will help develop low-cost TARs for domestic and business applications.

Wantha [17] tested a thermoacoustic refrigerator and simulated the effect of mean pressure of three types of geometric shapes on temperature of the cold side of the stack. The results show that the mean pressure of helium has an important influence on the temperature of the cold side and corresponds to the thermal penetration depth, so the temperature of the cold side of the stack is better. Finally, the cold side temperature of the pin array stack is reduced by about 70% compared to the cold side temperature of the circular pore stack, and the cold side temperature of the spiral stack is reduced by about 63%.

Chaiwongsa and Wongwises [18] conducted an experimental study on the performance of ASWTAR. Both heat exchangers of the refrigerator system used heat pipes. All relevant components of the thermoacoustic refrigerator had been fully used in the system, thus obtaining complete data on the cold side temperature, temperature difference, cooling load, and acoustic power. Finally, the data were used to determine the COP and COPR of the system.

As mentioned above, the performance of thermoacoustic refrigerator systems has been continuously improved. Air may not be used in actual refrigerators due to its low specific heat ratio and high Prandtl number. In any case, air can be used to study the effects of interdependent parameters. Nowadays, despite the low cost and reliable manufacturing process of air-based thermoacoustic refrigerators, its research has not attracted much attention [16,18]. The novelty of the work is the use of circular stack in a thermoacoustic refrigerator. Spiral stack has been popularly used in thermoacoustic refrigerator while the circular stack has never been studied. The results from comparison of both stacks may guide to the development of this kind of refrigerator. Therefore, the purpose of this study is to introduce ASWTAR. The effects of stack geometry, blockage ratio, and cooling power on COP and COPR are given. Both

λ	wavelength (m)
μ	dynamic viscosity (kg s^{-1} m^{-1})
ν	kinematic viscosity (m^2 s^{-1})
ρ_m	mean density (kg m^{-3})
σ	Prandtl number (dl)
ω	angular frequency (rad s^{-1})
ΔT_m	temperature difference (°C)
ΔT_{mn}	normalized temperature difference (dl)

heat exchangers of this system use heat pipes because of its simple installation, simple structure, less flow obstruction and high thermal efficiency. In addition, the performance of ASWTAR in circular stacks with different blockage rates is also introduced. Finally, the stack materials used in this study have better properties than those used in the previous work.

2. Experimental setup and procedure

ASWTAR was experimentally studied. Air is used as an operating gas in the test. The schematic diagram of the experimental setup is shown in Fig. 1. Thermoacoustic refrigerators are designed and optimized for quarter-wavelength ($\lambda/4$) resonator tubes. The components of a thermoacoustic refrigerator system are acoustic drivers, resonator tubes and cones, stacks, hot-side heat exchangers (HHX) and cold-side heat exchangers (CHX), and wave reflectors. Fig. 2 shows structural parameters of ASWTAR and dimensions of the resonator tube and stack, and Table 1 shows values of the structural parameters of the system. In general, the components are described in detail below.

Acoustic driver is a commercial loudspeaker with a maximum power of 150W at 8 Ω impedance and a driver diameter of 152 mm. The resonator cone is a truncated cone, made of aluminum plate, with a base diameter of 152 mm, and cone height of 40 mm. The resonator tube is made of 5 grades of PVC tubes, the resonator length (L_t) is 400 mm, and the inner diameter (D_r) is 56 mm. The stack geometry is spiral and circular, and the length (L_s) is 55 mm. The spiral stack is made of Mylar plates and separated by a nylon thread. Its thickness ($2l_0$) is 0.18 mm and the spacing ($2y_0$) is 0.5 mm. The circular stack is made of polylactic acid (PLA) and made by 3D printing with a thickness of 0.25 mm. The stack spacing and blockage ratios used in the experiment are shown in Table 2. The stack is installed in a resonator tube with the stack at the center position (X_s) of a 57.5 mm from the wave reflector.

The cold-side heat exchanger consists of an HPs holder made of a short PVC tube, a heat sink made of copper plates with dimensions of 40 × 40 × 3.5 mm (WxLxH), and 10 heat pipes (HPs) with a diameter of 2 mm. The length is 130 mm. The total heating power of 10 HPs CHX is about 30W. The complete CHX device is made by connecting 10 HPs between the heat sink and the holder with the same diameter as the resonator tube [18]. A square surface of the heat sink is milled with 10 parallel narrow slots so that the HP evaporator part is tightly fixed. In addition, the opposite surface of the heat sink is for a smooth joining of the thermoelectric hot surfaces. The HP condenser part is drilled through the holder and inserted transversely. The holder has been completely installed in the resonator tube. After that, the condenser part of HP should be close to the cold side of the stack.

The hot-side heat exchanger consists of a holder made of short PVC pipes, a cooling air duct with a diameter of 40 mm and a length of 150 mm, and 10 HPs with a diameter of 2 mm and a length of 130 mm. The total heating power of 10 HPs CHX is about 30W. The

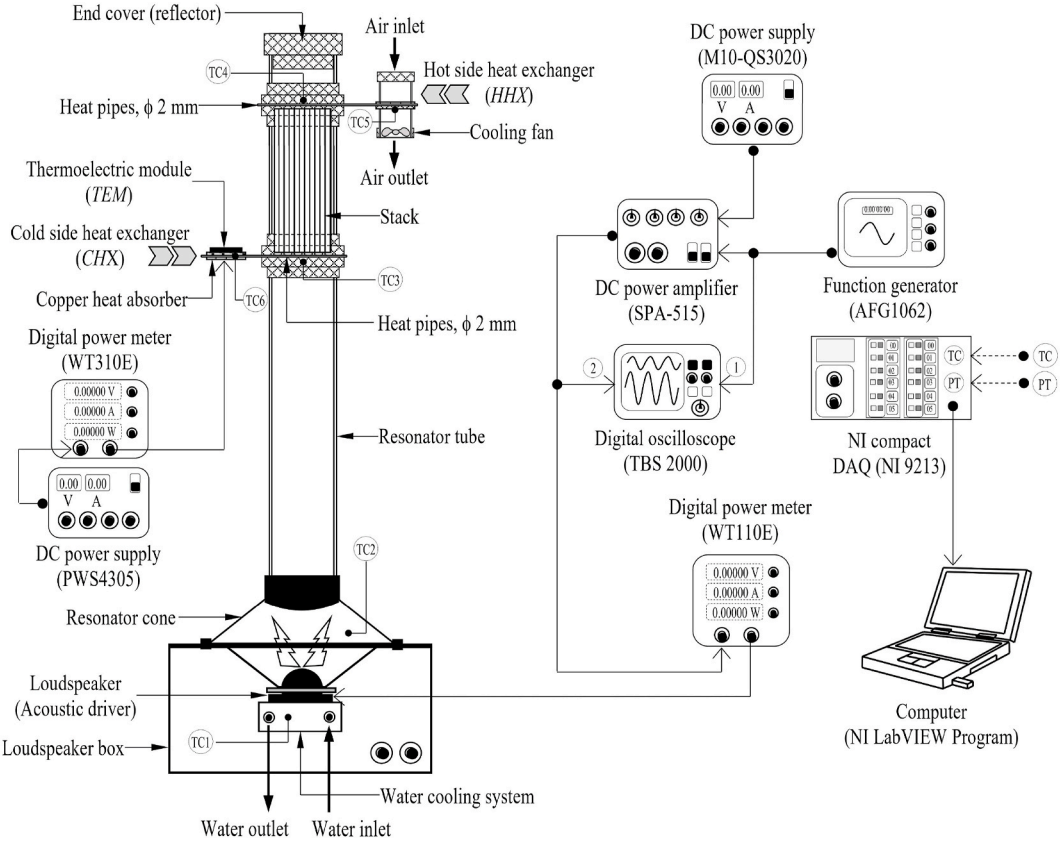

Fig. 1. Schematic diagram of experimental apparatus.

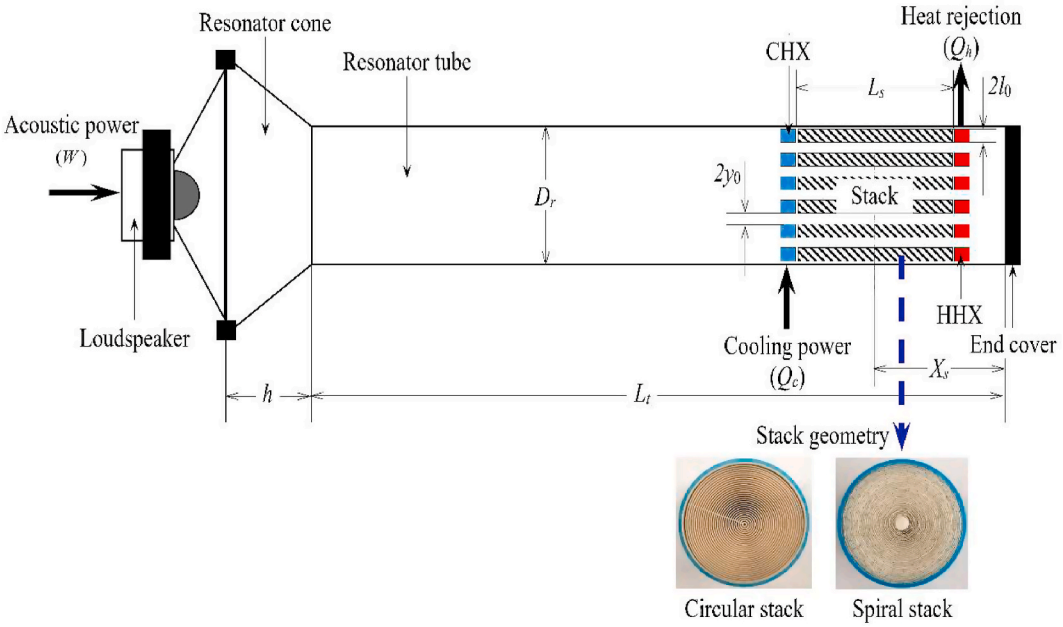

Fig. 2. Structure parameters of the ASWTAR.

Table 1
The structure and dimensions of the ASWTAR.

Structure	Symbol	Value	Unit
Resonator tube			
Diameter	D_r	56	mm
Thickness	–	1.8	mm
Length	L_t	400	mm
Material	PVC tube		
Resonator cone			
Base diameter	–	152	mm
Height	h	40	mm
Material	aluminum plate		
Stack			
Length	L_s	55	mm
Center position	X_s	57.5	mm
Geometry	spiral and circular shaped		
Material	Mylar and PLA		
Acoustic driver			
Material	commercial loudspeaker		
Cone diameter	–	152	mm
Impedance	–	8	Ω
Maximum power	–	150	W
Cold side heat exchange	CHX		
Material	heat pipe		
Total heating power	–	30	W
Heating device	TEM		
Hot side heat exchanger	HHX		
Material	heat pipe		
Total heating power	–	30	W
Cooling device	electric fan		

complete HHX set is made by connecting 10 HPs with a cooling duct and a holder. The cooling duct is a short cylinder used to cool HPs. The air inlet and outlet are connected at both ends. The condenser part of the HPs is inserted into the middle of the air duct, which hinders the flow direction of the cooling air when the electric fan flows. In the same way as CHX, the HP evaporator part is inserted into the holder, close to the hot side of the stack. The holder of HHX has been completely installed in the resonator tube. The HHX is used to absorb heat from the operating fluid near the hot side of the stack. The heat is then discharged to the environment through the cooling air in the duct.

The heat pipe used in the heat exchanger is a conventional composite wick type heat pipe, which is made from copper tube. A small

Table 2
Design parameters of stack for experiment.

Parameters	Symbol	Stack geometry				Unit
		Circular			Spiral	
stack material	–		PLA		Mylar	
stack thickness	$2l_0$		0.25		0.18	mm
thermal penetration depth	δ_k		0.217		0.217	mm
stack spacing	$2y_0$	0.5	0.6	0.7	0.5	mm
		$2.3\delta_k$	$2.8\delta_k$	$3.2\delta_k$	$2.3\delta_k$	
blockage ratio	B	0.67	0.71	0.74	0.74	
heat transferring surface area	A_s	0.37	0.33	0.29	0.4	m^2

diameter copper wire is inserted into the pipe. Deionized water is used as the operating fluid, as shown in Table 3.

T-type thermocouple (accuracy of ±0.1 °C) is used to measure the temperature of ASWTAR at various locations and is connected to a compact DAQ system (module: 9213, NI), and evaluated in a computer through a LabVIEW program. Dry well calibrator (model: 9103, Fluke) has a temperature range of −25 °C to +140 °C and an accuracy of ±0.25 °C, which is used to calibrate thermocouples.

Instruments used in acoustic wave generation and measurement include: function generator (model: AFG1062, Tektronix), whose sinusoidal signal frequency range is 1 μHz to 60 MHz; digital oscilloscope (model: TBS2000, Tektronix), with 0–100 MHz Bandwidth and four analog channels, an amplifier (model: SPA-515, Schneider) with a maximum output power of 150W at 8 Ω impedance, and a DC power supply (model: M10-QS3020, MCP) with a maximum of 20A current and output voltage range of 0–30 V, and two digital power meters: i) Cooling load: power meter (model: WT310E, Yokogawa), input current range is 0–5A, the input voltage range is 0–15 V, ± (0.1% of reading +0.2% of range) accuracy in DC, ii) Acoustic input power: power meter (model: WT110E, Yokogawa), input current range 0–5A, input voltage range 0–30 V, ± (0.2% of reading + 0.2% of range) accuracy.

The test uses a function generator to adjust the acoustic power and set the operating frequency. A digital oscilloscope is used to observe the frequency of system. A digital power meter is used to measure acoustic power. The heat of TEM is used as the cooling load of the refrigerator. A DC power supply (model: PWS4305, Tektronix) is used to control the cooling load by adjusting the voltage supplied to the TEM. A digital power meter (model: WT310E, Yokogawa) is used to measure the cooling power of the system.

Tests are conducted to estimate the resonant frequency of the ASWTAR with the circular stack. The blockage ratio of circular stack is 0.67, 0.71, and 0.74. If there is no cooling load, the required frequency varies from 120 to 190 Hz. Each trial step is 10 Hz. 20W of electrical input power is supplied under all conditions.

As shown in Table 2, tests are conducted to estimate the COP of ASWTAR for circular stacks with blockage ratios of 0.67, 0.71, and 0.74 and spiral stacks with a blockage ratio of 0.74. For the test, the cooling load is changed by adjusting the cooling load. Voltage is supplied to the TEM installed in the CHX. The initial cooling load varies from 0 to 2W in steps of 0.5W. The acoustic power of the-cooling load is changed by adjusting the power provided to the acoustic driver.

The resonant frequency of 150 Hz is used as the desired frequency and kept constant in all experiments. A compact DAQ system is used to record test data, by connecting it to a computer, and collecting data under steady-state conditions. Tests are varied by adjusting various acoustic power, frequency, and cooling load. For each test, a cooling system is used to dissipate the heat from the loudspeaker voice coil to bring its temperature close to the ambient temperature.

3. Data reduction

The working principle of thermoacoustic refrigeration is to use the acoustic work to force the gas parcels to flow through a porous medium (so-called “stack”) so that the compressed gas particles transfer heat to the stack surface and the stack surface dissipate heat into the expanding gas particles. This process occurs continuously and rapidly according to the resonant frequency of the sound wave. The temperature gradient of the entire stack is obtained. Consequently, the heat can be transferred from the cold side to the hot side of the stack through the acoustic work. This phenomenon is called the “thermoacoustic effect”.

Acoustic drivers, resonator tubes, stacks, and heat exchangers are the basic components of thermoacoustic refrigerators. The main structure of a refrigerator equipped with all other components is a resonator tube. The resonator of the acoustic wave appears inside the tube. The acoustic driver generates acoustic waves into the resonator tube in a standing waveform. The stack is installed in the

Table 3
Structure parameters of heat pipe heat exchanger (HPHX).

Parameters	CHX	HHX
type of heat pipe	composite wick	composite wick
tube size	ϕ2x130 mm	ϕ2x130 mm
tube wall	smooth	smooth
wick	capillary wires	capillary wires
material	copper	copper
working fluid	deionized water	deionized water
heating power	3 × 10 W	3 × 10 W

pressure amplitude region inside the resonator tube. This causes the resonator to experience thermoacoustic effects. Therefore, the stack is considered to be the most important equipment in the thermoacoustic refrigeration system.

Heat exchangers installed near the two ends of the stack are used to absorb and remove heat from the system. Since it is a low thermal conductivity material, the resonator tube used in this study is made of a PVC tube, so the heat loss due to conduction is low. Hofler [2] suggested setting the appropriate length parameter of the resonator tube design to λ/4. A large amount of heat conduction of gas through the surface of the stack is avoided because it reduces the performance of the refrigerator [3]. Stackmaterials with high specific heat and low thermal conductivity are required for heat transfer on the stack surface. However, due to the low thermal conductivity of air, the thermal penetration depth and stack spacing are small-sized.

Table 4 shows the materials and properties of the stack. Mylar and PLA materials were chosen because of their higher specific heat and lower thermal conductivity, and their thicknesses of 0.18 and 0.25 mm. In addition, other instruments of the refrigerator are function generators, power amplifiers, power meters, oscilloscopes, thermocouples, and DAQ systems. The necessary data for designing ASWTAR and the thermodynamic properties of the operating fluid under STP conditions are shown in Table 5.

In the system design, some parameters are used to consider, for example, operating frequency, hot side temperature, cold side temperature and required cooling power. To avoid turbulent flow, the Reynolds number, Re, is kept below 500 [13], defined as

$$Re = \frac{u\delta_v}{\nu}. \tag{1}$$

In order to protect nonlinear effects, an acoustic Mach number, M, is limited not to exceed 0.1 [13]. The drive ratio, D, is computed by

$$D = \frac{p_0}{p_m} = \frac{M\rho_m a^2}{p_m} \tag{2}$$

D of 0.02 was chosen to meet the conditions of Re < 500 and M < 0.1 [9]. The stack spacing is considered based on two properties: viscous penetration depth, δ_v, which is determined by

$$\delta_v = \sqrt{\frac{2\mu}{\rho_m \omega}}. \tag{3}$$

and thermal penetration depth, δ_k, which is determined by

$$\delta_k = \sqrt{\frac{2k}{\rho_m c_p \omega}}. \tag{4}$$

In the above equations, ν is kinematic viscosity, u is axial velocity, p_m is mean pressure, p_0 is dynamic pressure, a is the speed of sound, μ is dynamic viscosity, ρ_m is mean density, c_p is the isobaric specific heat of the gas, k is thermal conductivity, and ω is the angular frequency of the sound wave. The angular frequency is defined as

$$\omega = 2\pi f. \tag{5}$$

The optimal stack spacing should be between $2\delta_k$-$4\delta_k$ [10]. In this study, the stack spacing is produced as 0.5–0.7 mm by considering the δ_k value.

In addition, the normalized acoustic power, W_n, and normalized cooling power, Q_{cn}, are expressed [2] as

$$W_n = \frac{W}{p_m a A} = \left\{\frac{\delta_{kn} D^2 L_{sn}(\gamma-1)B\cos^2(X_{sn})}{4\gamma}\right\} \times \left\{\left(\frac{\Delta T_{mn}\tan(X_{sn})}{BL_{sn}(\gamma-1)\left(1+\sqrt{\sigma}\right)\left(1-\sqrt{\sigma}\,\delta_{kn}+\frac{1}{2}\sigma\delta_{kn}^2\right)}\right)-1\right\}$$
$$-\left\{\frac{\delta_{kn}L_{sn}D^2}{4\gamma}\times\frac{\sqrt{\sigma}\sin^2(X_{sn})}{B\left(1-\sqrt{\sigma}\,\delta_{kn}+\frac{1}{2}\sigma\delta_{kn}^2\right)}\right\} \tag{6}$$

and

Table 4
Properties of stack materials for experiment.

Properties	Symbol	Mylar	PLA	Unit
density	ρ	1347.5	1300	kg m^{-3}
thermal conductivity	k	0.16	0.13	W m^{-1} K^{-1}
specific heat of stack	c_s	1110	1800	J kg^{-1} K^{-1}

Table 5
Thermophysical properties of working gas and design parameters.

	Symbol	Value	Unit
Working gas properties			
Prandtl number	σ	0.707	
ratio of specific heat	γ	1.4	
speed of sound	a	347.2	$m\ s^{-1}$
thermal conductivity	k	0.026	$W\ m^{-1}\ K^{-1}$
mean density	ρ_m	1.161	$kg\ m^{-3}$
isobaric specific heat	c_p	1007	$J\ kg^{-1}\ K^{-1}$
Design parameters			
mean pressure	p_m	101.33	kPa
mean temperature	T_m	300	K
mean temperature difference	ΔT_m	25	K
normalized stack position	$X_{sn} = KX_s$	0.156	
normalized stack length	$L_{sn} = KL_s$	0.149	
normalized thermal penetration depth	σ_{kn}	0.181	
wave number	K	2.895	m^{-1}
operating frequency	f	150	Hz
drive ratio	D	0.004	
blockage ratio	B	0.71	
ambient temperature	–	28	°C

$$Q_{cn} = \frac{Q_c}{p_m a A} = -\left\{\frac{\delta_{kn} D^2 \sin(2X_{sn})}{8\gamma(1+\sigma)\left(1-\sqrt{\sigma}\,\delta_{kn}+\frac{1}{2}\sigma\delta_{kn}^2\right)}\right\} \times \left\{\frac{\Delta T_{mn}\tan(X_{sn})}{(\gamma-1)BL_{sn}} \times \frac{1+\sqrt{\sigma}+\sigma}{1+\sqrt{\sigma}} - \left(1+\sqrt{\sigma}-\sqrt{\sigma}\ \delta_{kn}\right)\right\}, \tag{7}$$

in Eqs. (6) and (7), Q_c, W, A, γ, σ and B represented, respectively, the cooling power, acoustic power, cross-sectional area of the stack, specific heat ratio, Prandtl number, and blockage ratio. The blockage ratio is the ratio of a cross-sectional area of the gas, A_g, and cross-sectional area of the stackexpressed by the equation

$$B = \frac{y_0}{y_0 + l_0}, \tag{8}$$

where l_0 is half of the stack thickness and y_0 is half of the stack spacing. The four normalized parameters that appeared in Eqs. (6) and (7) are dimensionless forms, which is an important factor in the thermoacoustic refrigeration. The normalized temperature difference, ΔT_{mn}, is a ratio of temperature difference, ΔT_m, and mean temperature, T_m, expressed as

$$\Delta T_{mn} = \frac{\Delta T_m}{T_m}. \tag{9}$$

The normalized thermal penetration depth, δ_{kn}, is defined as

$$\delta_{kn} = \frac{\delta_k}{y_0}. \tag{10}$$

The normalized stack center position, X_{sn}, and normalized stack length, L_{sn}, are defined as

$$X_{sn} = \frac{2\pi f}{a} X_s \tag{11}$$

and

$$L_{sn} = \frac{2\pi f}{a} L_s \tag{12}$$

where X_s is the distance from half the stack length to the wave reflector and L_s is stack length.

In Eq. (7), many parameters seem to affect the cooling power. However, some parameters are constant (for example, the blockage ratio and geometry of the stack). It can be recognized that the important parameters are operating frequency, average pressure, average temperature, hot-side temperature, and drive ratio [13]. However, the drive ratio is only a small part of the pressure. Finally, cooling power is the main function of the inevitable mean pressure, mean temperature and frequency. Therefore, Q_c can be expressed as

$$Q_c = Q_c(p_m,\ T_m,\ f\ ). \tag{13}$$

Tests were conducted to study the effect of cooling power, frequency, and blockage ratio on thermoacoustic refrigeration. Generally, the efficiency of a refrigerator is explained by the coefficient of performance COP, which is defined as

$$COP = \frac{Q_{cn}}{W_n} = \frac{Q_c}{W}. \quad (14)$$

The Carnot's coefficient of performance, COPc, which is the maximal COP of the refrigerating system, determined by

$$COPc = \frac{T_c}{T_h - T_c}, \quad (15)$$

when T_c is the cold side temperature and T_h is the hot side temperature. The relative coefficient of performance, COPR, which is a comparison of performance between the system and Carnot's, defined as

$$COPR = \frac{COP}{COPc}. \quad (16)$$

The uncertainties of the experimental parameters are shown in Table 6.

4. Results and discussion

4.1. Resonant frequency

Fig. 3 shows that for a circular stack with a blockage ratio of 0.67, 0.71 and 0.74, the cold side temperature (T_c) varies with the operating frequency at an input power of 20W. The graph shows that at first stage, as the operating frequency increases, T_c will decrease. At an operating frequency of 150 Hz, T_c drops to a minimum and then begins to increase as the frequency increases. This is because under the optimal operating conditions of the system, the maximum pressure amplitude and thermoacoustic effects will occur at the resonant frequency. Therefore, the heat pumping used to transfer heat from the cold side end (CSE) of the stack to the hot side end (HSE) at the resonant frequency is higher than other frequencies. It can be clearly seen from the graph that T_c is the lowest at the frequency of 150 Hz. The blockage ratio (B) of the circular stack with the lowest, second-lowest and highest T_c are found to be 0.71, 0.74, and 0.67, respectively. This is because when the B is 0.71, the friction loss is smaller than that at the other blockage ratios. Therefore, there are more heat pumps on the cold end, which ultimately produces the lowest T_c.

4.2. Electric input voltage

Fig. 4 shows that for circular stack with a blockage ratio of 0.67, 0.71 and 0.74, the input voltage varies with the operating frequency at 20W input power. The graph shows that at the first stage the input voltage will increase as the operating frequency increases. The input voltage increases to the maximum value when the operating frequency is 150 Hz, and then decreases when the operating frequency increases. This is because, when the operating frequency reaches the resonant frequency, the thermoacoustic effect becomes more intense.

Electrical input power (P_i) is the power supplied to the acoustic driver to be converted into acoustic power. It can be calculated according to $P_i = E_i \times I_i \times PF$, where E_i is the input voltage, I_i is the input current and PF is the power factor. On the other hand, the acoustic power (W) is the power used for the heat pumping in the thermoacoustic refrigerator, which can be calculated from $W = \eta_s \times P_i$, where η_s is the electroacoustic conversion efficiency. The efficiency of the loudspeaker used for the calculation in this study was 8%. The efficiency of the loudspeaker can be considered from the sensitivity level of the loudspeaker, which can be tested by the manufacturer, and calibrated by the efficiency and sensitivity level conversion chart. As can be seen from Fig. 4, the blockage ratio of the circular stack with the highest input voltage, the second-highest and the lowest is 0.71, 0.74 and 0.67, respectively. This is because when the friction of the operating gas discharged through the acoustic waves in the resonator tube is reduced, the acoustic driver will consume less current while maintaining a stable input power. Therefore, the electrical input voltage increases and causes the pressure amplitude of the acoustic wave and the thermoacoustic effect of the system to increase. Therefore, the main factor is the reduction of acoustic power loss.

According to Ohm's law, at constant electrical power, the voltage varies inversely with the current. That is, as the current increases, the voltage will decrease. In other words, when the electrical resistance of the system is higher, the current will increase. The electric current affects electrical device, causing heat and heat losses. Therefore, according to Fig. 4, an increase in the electrical input voltage of the system indicates that the resistance of the system decreases.

However, in this study, the operating frequency with the highest electrical input voltage is considered. This operating frequency

Table 6
The uncertainties of the experimental parameters.

Parameters	Uncertainty (%)
Temperature difference (ΔT_m)	±0.46
Cooling load (Q_c)	±2.65
Acoustic power (W)	±1.03
COP	±2.85
COPc	±0.46
COPR	±2.89

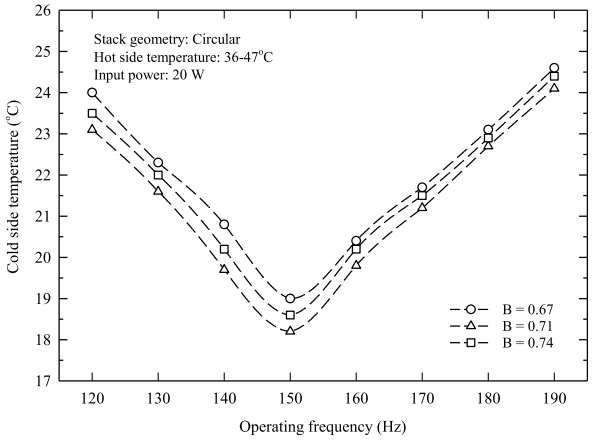

Fig. 3. Comparison of cold side temperature and operating frequency for circular stack with different blockage ratio at input power of 20 W.

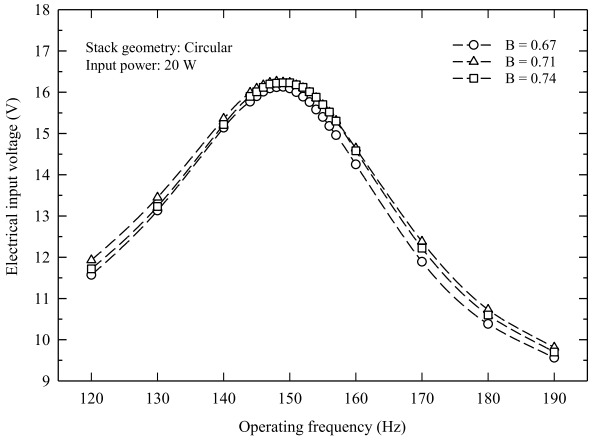

Fig. 4. Comparison of electrical input voltage and operating frequency for circular stack with different blockage ratio at input power of 20 W.

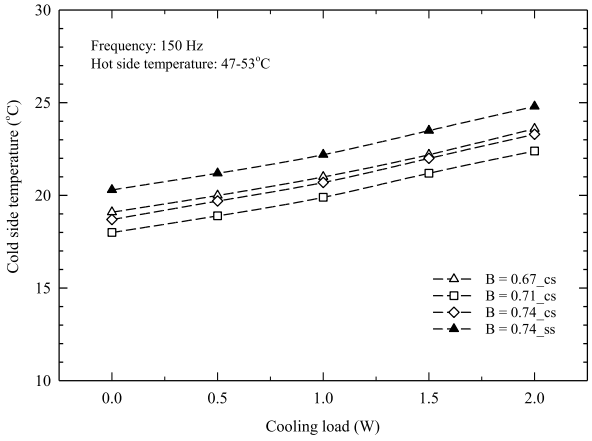

Fig. 5. Comparison of cold side temperature and cooling load for spiral and circular stack at different blockage ratio.

having the minimum friction of acoustic waves may be an indicator of the resonant frequency of the system. Therefore, the resonant frequency of the system is the operating frequency of 150 Hz.

4.3. Cold side temperature (T_c)

Fig. 5 shows the change of the cold side temperature with the cooling load at an operating frequency of 150 Hz. The blockage ratio (B) of the circular stack is 0.67, 0.71, and 0.74, and the blockage ratio of the spiral stack is 0.74. The graph shows that as the cooling load (Q_c) increases, the cold side temperature (T_c) will increase with a constant slope. This is because the acoustic driver is inefficient. Therefore, the acoustic power for heat pumping from the cooling load is also very low. As a result, the system cannot maintain constant T_c. Therefore, as Q_c increases, the system's T_c also increases. When comparing the T_c and B of the stack, the B of the circular stack with the lowest, second-lowest, and highest T_c is found to be 0.71, 0.74, and 0.67. When $Q_c = 0$W, T_c equals 18, 18.7, and 19.1 °C; when $Q_c = 2$W, T_c equals 22.4, 23.3, and 23.6 °C, respectively. Since the stack spacing ($2y_0$) is related to thermal penetration depth (δ_k), $2y_0$ is $2\delta_k$ - $4\delta_k$ as suggested by Refs. [3,9]. The circular stack spacing used in this study is $2.3\delta_k$, $2.76\delta_k$, and $3.22\delta_k$, which are equal to 0.5, 0.6, and 0.7 mm, respectively. Therefore, B is 0.67, 0.71 and 0.74, respectively. In addition, from the design of the circular stack, it is also found that the heat transfer surface area (A_s) of the circular stack with B of 0.67, 0.71, and 0.74 is 0.37, 0.33, and 0.29 m^2, respectively. Therefore, the optimal design parameters for the circular stack with the lowest T_c are $B = 0.71$, $2y_0 = 2.7\delta_k = 0.6$ mm, $2l_0 = 0.25$ mm, $L_s = 55$ mm, $X_s = 57.5$ mm, and $A_s = 0.33$ m^2. In addition, when comparing the T_c and stack geometry, it is found that the T_c for all B of circular stacks is lower than that of the spiral stack with $B = 0.74$. This is because the circular stack is made of PLA material, while the spiral stack is made of Mylar material. When examining the thermal conductivity (k) and specific heat (c_s) of the material, it is found that PLA has a lower k and a higher c_s than Mylar. It can be clearly seen that PLA is a more suitable material for stacking than Mylar. Therefore, the heat transfer from the CSE to the HSE of the circular stack is higher than the spiral stack. At $Q_c =$ 0W and 2W, the T_c of the spiral stack with $B = 0.74$ is 20.3 and 24.8 °C, respectively.

4.4. Temperature difference (ΔT_m)

Fig. 6 shows variations of temperature difference along with cooling load at an operating frequency of 150 Hz for circular stacks with B of 0.67, 0.71 and 0.74, and spiral stack with B of 0.74. At the beginning, the increase of T_c is less than the increase of T_h. This results in the increase of ΔT_m, and the thermoacoustic heat pumping, which is a mechanism to transport the heat from the cold end to the hot end of the stack, is higher. As a result, the cooling load increases with an increase in ΔT_m. However, when the cooling load is around 1.5 W, the increase of T_c is more than the increase of T_h which results in the decrease of ΔT_m and the rate of thermoacoustic heat pumping. Finally, ΔT_m tends to decrease as the cooling load increases.

When comparing ΔT_m and B of the stack, it is found that the B of circular stack with the highest, the second-highest and the lowest ΔT_m are 0.71, 0.74, and 0.67. When $Q_c = 0$W, ΔT_m is equal to 29, 28.3 and 27.9 °C, and when $Q_c = 2$W, ΔT_m is equal to 30.5, 29.6 and 29.3 °C, respectively. In addition, when comparing ΔT_m and stack geometry, it is found that for all B, the ΔT_m of the circular stack is higher than that of the spiral stack with $B = 0.74$. When $Q_c = 0$W and 2W, the ΔT_m of the spiral stack with $B = 0.74$ is equal to 26.7 and 28.1 °C, respectively.

4.5. Coefficient of performance (COP)

Fig. 7 shows the change in COP with a cooling load at an operating frequency of 150 Hz. The B of the circular stack is 0.67, 0.71, and 0.74, and the B of the spiral stack is 0.74. The graph shows that as the cooling load increases, the COP will increase. This is because when the system has no cooling load ($Q_c = 0$W), the work provided to the system in the form of acoustic energy will become heat. The heat generated by the work will be extracted to make the system enter a steady state. Therefore, when a cooling load is received, the system needs more acoustic power to extract the heat from the cooling load and return to a steady-state. As a result, the acoustic power used under high cooling loads is less than the acoustic power used under low cooling loads leading to an increase in the COP of the system. When comparing the COP and B of the stack, it is found that when $Q_c = 2$W, the highest, second, and lowest COP of the circular stack are 0.93, 0.91, and 0.9, and B is 0.71, 0.74, and 0.67, respectively. In addition, when comparing the COP and stack geometry, it is found that the COP of a circular stack is higher than that of a spiral stack. This is because the circular stack used in this study is made from Polylactic acid (PLA), while the spiral stack is made of Mylar. Usually, the PLA has lower thermal conductivity but higher specific heat than the Mylar. The low thermal conductivity of stack causes more difficulty in transferring heat to the stack, thus allowing more heat transfer through the air than to the stack. The high specific heat of the stack makes the stack absorb heat from the air. Therefore, the circular stack absorbs more heat but provides less heat loss than the spiral stack. The circular stack gives less heat loss in process than a spiral stack which causes less acoustic power with constant cooling capacity. This ultimately results in a higher COP of the circular stack than the spiral stack although the heat transfer surface area of the spiral stack is higher than that of the circular stack.

4.6. Relative coefficient of performance (COPR)

Fig. 8 shows the variations in COPR and cooling load at an operating frequency of 150 Hz, where for circular stacks, B is 0.67, 0.71, and 0.74, and for spiral stacks, B is 0.74. The graph shows that as the cooling load increases, the COPR will increase. This is because the increase in cooling load causes Carnot's coefficient of performance (COPc) to decrease; therefore, the system's COPR increases. When comparing the COPR and B, it is found that when $Q_c = 2$W, the B of the circular stack with the highest, second-highest, and lowest

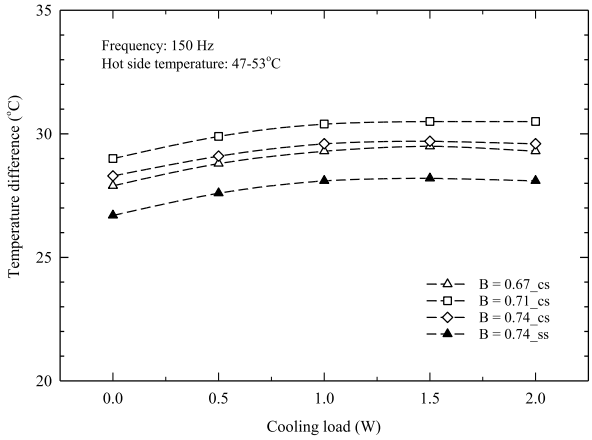

Fig. 6. Comparison of temperature difference and cooling load for spiral and circular stack at different blockage ratio.

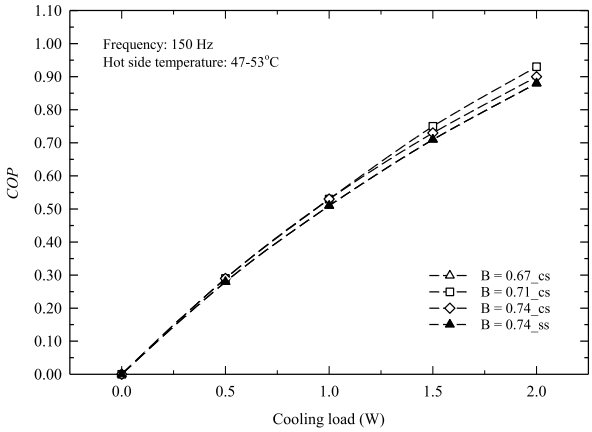

Fig. 7. Comparison of COP and cooling load for spiral and circular stack at different blockage ratio.

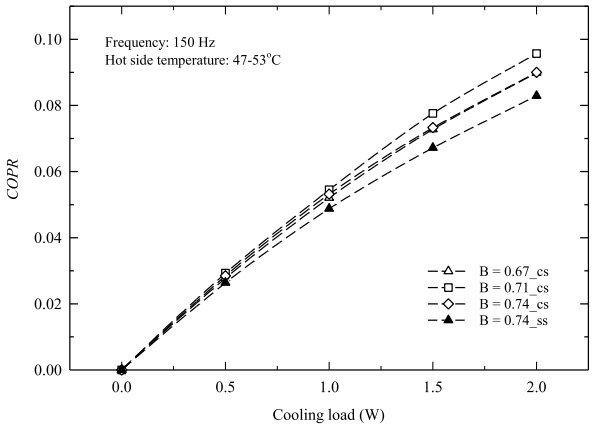

Fig. 8. Comparison of COPR and cooling load for spiral and circular stack at different blockage ratio.

COPR of 9.57%, 9%, and 8.99% was 0.71, 0.74, and 0.67, respectively. In addition, when comparing the COPR and stack geometry, it is found that the slope of all COPR of a circular stack is higher than that of a spiral stack. When $Q_c = 2W$, the maximum COPR of the spiral stack is 8.29%.

However, when the actual COP of the system is the same, a system with a higher COPR can still make full use of heat at a higher ratio. Therefore, it can be said that even in the case of the same or higher system actual COP, the system with higher COPR can run

better than the system with lower COPR, which is consistent with the second law efficiency.

5. Conclusion

The performance of ASWTAR was studied. A PVC resonator tube with an inner diameter of 56 mm and an aluminum resonator cone with a cone-base diameter of 152 mm are tested and compared. The experiment is also tested with various stacking geometries. The stack is made from Mylar and PLA material. A spiral stack with a blockage ratio of 0.74 and a circular stack with a blockage ratio of 0.67, 0.71, and 0.74 is also studied and compared. HPs with a total heating power of 30W are installed on the CHX and the HHX. The cooling loads are heat transferred from the TEM by connecting the hot side of the TEM to the heat absorber and transferring the heat to the CHX through HPs. The HP is used to dissipate heat from the system via HHX, and then a cooling fan is used to transfer it to the environment. The maximum cooling load of ASWTAR is 2W. In order to carry out the experiment, a test is conducted with an operating frequency of 120–190 Hz and an electrical input power of 20W without a cooling load. Thereafter, the system is supplied with heat from the TEM with cooling loads of 0.5, 1, 1.5, and 2W and a resonant frequency of 150 Hz.

In the case of no cooling load, 20W input power, and 120–190 Hz operating frequency, the results show that the circular stack with a blockage ratio of 0.67, 0.71 and 0.74 gives the minimum T_c and produces the maximum E_i. At this time, this is the best state of the thermoacoustic refrigerator. So far, the optimal resonant frequency of the system is 150 Hz.

At a cooling load with a frequency of 150 Hz, the results show that when a circular stack with blockage ratios of 0.67, 0.71, and 0.74 and a spiral stack with blockage ratio of 0.74, T_c increases while the cooling load increases. Also, a constant slope is observed. In addition, a circular stack with a blockage ratio of 0.71 gives the lowest T_c and the highest ΔT_m. At a cooling load of 0W, T_c and ΔT_m are 18 and 29 °C, respectively. Similarly, at a cooling load of 2W, for a circular stack with a blockage rate of 0.71, T_c and ΔT_m are 22.4 and 30.5 °C, respectively, COP and COPR are 0.93 and 9.57%, respectively. For the circular stack, the design parameters with the optimum points, including B, $2y_0$, $2l_0$, L_s, X_s, and A_s are 0.71, 0.6 mm, 0.25 mm, 55 mm, 57.5 mm, and 0.33 m^2, respectively. In addition, the results show that the circular stack has higher COP and COPR than the spiral stack at all blockage ratios. Finally, under a cooling load of 2W, the COP and COPR of the spiral stack are about 0.88 and 8.92%, respectively.

CRediT authorship contribution statement

Praitoon Chaiwongsa: Experiment, Investigation. **Somchai Wongwises:** Investigation, Writing - original draft, Writing - review & editing.

Declaration of competing interest

The authors declare that they have no known competing financial interests or personal relationships that could have appeared to influence the work reported in this paper.

Acknowledgement

The authors acknowledge the support provided by the “Research Chair Grant” National Science and Technology Development Agency (NSTDA), the Thailand Science Research and Innovation (TSRI) and the KMUTT 55th Anniversary Commemorative Fund.

References

[1] N. Rott, Thermoacoustics, Adv. Appl. Mech. 20 (1980) 135–175.
[2] T.J. Hofler, Thermoacoustic Refrigerator Design and Performance, University of California, San Diego, CA, 1986 (Ph.D. thesis).
[3] G.W. Swift, Thermoacoustic engines, J. Acoust. Soc. Am. 84 (4) (1988) 1145–1180.
[4] S.L. Garrett, J.A. Adeff, T.J. Hofler, Thermoacoustic refrigerator for space applications, J. Thermophys. Heat Tran. 7 (4) (1993) 595–599.
[5] G.W. Swift, Thermoacoustic engines and refrigerators, Phys. Today 48 (7) (1995) 22–28.
[6] M. Wetzel, C. Herman, Design optimization of thermoacoustic refrigerators, Int. J. Refrigeration. 20 (1) (1997) 3–21.
[7] J.R. Belcher, W.V. Slaton, R. Raspet, H.F. Bass, J. Lightfoot, Working gases in thermoacoustic engines, J. Acoust. Soc. Am. 105 (5) (1999) 2677–2684.
[8] M.E. Poese, S.L. Garrett, Performance measurements on a thermoacoustic refrigerator driven at high amplitudes, J. Acoust. Soc. Am. 107 (5) (2000) 2480–2486.
[9] M.E.H. Tijani, J.C.H. Zeegers, A.T.A.M. de Waele, Construction and performance of a thermoacoustic refrigerator, Cryogenics 42 (2002) 59–66.
[10] M.E.H. Tijani, J.C.H. Zeegers, A.T.A.M. de Waele, Design of thermoacoustic refrigerators, Cryogenics 42 (2002) 49–57.
[11] C. Herman, Y. Chen, A simplified model of heat transfer in heat exchangers and stack plates of the thermoacoustic refrigerators, Heat Mass Tran. 42 (2006) 901–917.
[12] M. Akhavanbazaz, M.H.K. Siddiqui, B.R. Bhat, The impact of gas blockage on the performance of a thermoacoustic refrigerator, Exp. Therm. Fluid Sci. 32 (2007) 231–239.
[13] E.C. Nsofor, A. Ali, Experimental study on the performance of the thermoacoustic refrigerating system, Appl. Therm. Eng. 29 (2009) 2672–2679.
[14] S.H. Tasnim, S. Mahmud, R.A. Fraser, Effects of variation in working fluids and operating conditions on the performance of a thermoacoustic refrigerator, Int. Commun. Heat Mass Tran. 39 (6) (2012) 762–768.
[15] B.R. Nayak, G. Pundarika, B. Arya, Influence of stack geometry on the performance of thermoacoustic refrigerator, Indian Acad. Sci. 42 (2) (2017) 223–230.
[16] S.G. Yahya, X. Mao, A.J. Jaworski, Experimental investigation of thermal performance of random stack materials for use in standing wave thermoacoustic refrigerators, Int. J. Refrigeration 75 (2017) 52–63.
[17] C. Wantha, The impact of stack geometry and mean pressure on cold end temperature of stack in thermoacoustic refrigeration systems, Heat Mass Tran. 54 (7) (2018) 2153–2161.
[18] P. Chaiwongsa, S. Wongwises, Experimental investigation on the performance of the air−based standing wave thermoacoustic refrigerator using heat pipe as heat exchangers, Int. J. Air Cond. Refrig. 28 (1) (2020) 52–63.